Soft template assisted self-assembly: a general strategy toward two-dimensional molecular crystals for high-performance organic field-effect transistors

Xinzi Tian,‡[a] Jiarong Yao,‡[a] Siyu Guo,‡[a] Zhaofeng Wang,[a] Yanling Xiao,[b] Heng Zhang,[c] Yiyu Feng,[c] Wei Feng,[c] Jiansheng Jie,[b] Fangxu Yang,[a] Rongjin Li*[a] and Wenping Hu[a]*

[a]Tianjin Key Laboratory of Molecular Optoelectronic Sciences, Department of Chemistry, School of Science, Tianjin University & Collaborative Innovation Center of Chemical Science and Engineering, Tianjin 300072, China.

[b]Institute of Functional Nano & Soft Materials (FUNSOM), Jiangsu Key Laboratory for Carbon-Based Functional Materials & Devices Soochow University, Suzhou 215123, China.

[c]School of Materials Science and Engineering, Tianjin University, Tianjin 300072, China

Email: yangfangxu@tju.edu.cn, lirj@tju.edu.cn

Contents

Fabrication of 2DMCs and their heterojunction

The 2DMCs were grown as follows: (i) 25 mL water with 0.02 mg mL^{-1} $C_8F_{17}KO_3S$ was added into a weighing bottle (70 mm × 35 mm) as a liquid substrate for crystal growth. (ii) C6-DPA with a concentration of 0.2 mg mL^{-1} was dissolved in a low surface tension solution (e.g., toluene) and 60 μL of C6-DPA solution was slowly dropped on the surface of water (Fig. S1a and S1b, ESI†). C6-DPA 2DMCs obtained by solutions of different concentrations were shown in Fig. S2a-b (ESI†). (iii) After the solvent was completely evaporated, C6-DPA 2DMCs were obtained on the surface of water (Fig. S1c, ESI†). (iv) SiO$_2$ (300 nm)/Si wafers were used as the substrates. They were cleaned by sonication in deionized water, acetone, and isopropanol for 10 min successively. Then the substrates were treated with oxygen plasma at 80 W for 10 min followed by immediately modification with octadecyltrichlorosilane (OTS) by a vapor phase method. (v) The as-grown C6-DPA 2DMCs were transferred to OTS-modified SiO$_2$/Si substrates by immersing the substrate in water (Fig. S1d, ESI†).

The bilayer heterojunctions based on C6-DPA and TFT-CN 2DMCs were constructed as follows: A toluene solution of TFT-CN with a concentration of 1 mg mL^{-1} was prepared and 60 μL of TFT-CN solution was slowly dropped on the surface of water with 0.02 mg mL^{-1} $C_8F_{17}KO_3S$. After the solvent was completely evaporated, TFT-CN 2DMCs were obtained. The as-grown TFT-CN 2DMCs were transferred to the substrates pre-covered by C6-DPA 2DMCs to form the heterojunctions.

In addition, 2DMCs of various organic materials can also be transferred to OTS-modified SiO$_2$/Si substrates by immersing the substrate in water and fishing the crystals out (Fig. S6-S9, ESI†), so that many types of bilayer heterojunctions can be easily obtained by arbitrarily combination of 2DMCs through a layer-by-layer transfer method (Fig. S12 and S13, ESI†).

Calculation of the layer numbers of C6-DPA and TFT-CN

According to XRD patterns of C6-DPA (Fig. S10, ESI†), we can infer that the *d*-spacing is 3.2 nm, which coincides with the length of a C6-DPA molecule along the long axis.[1] A monolayer 2DMC of C6-DPA was about 2.9 nm measured by AFM.[2] As a result, we calculated the layer number of C6-DPA as follows: n = (T-2.9)/3.2+1 (n was layer

number, T was the thickness of C6-DPA obtained by AFM. As shown in Fig. 2b, the thickness of C6-DPA 2DMCs was 8.4 nm. By substituting the thickness of C6-DPA into the above formula, the number of layers was three. As for TFT-CN, according to the XRD (Fig. S11, ESI†) and the single crystal structure,[3] a monolayer thickness was 1.6 nm. As a result, we calculated the layer number of TFT-CN as follows: n = T/1.6 (n was layer number, T was the thickness of TFT-CN obtained by AFM). Considering the possibility that the first monolayer may tilt in a bilayer film, we think a film with a thickness of 2.5 nm is bilayer.
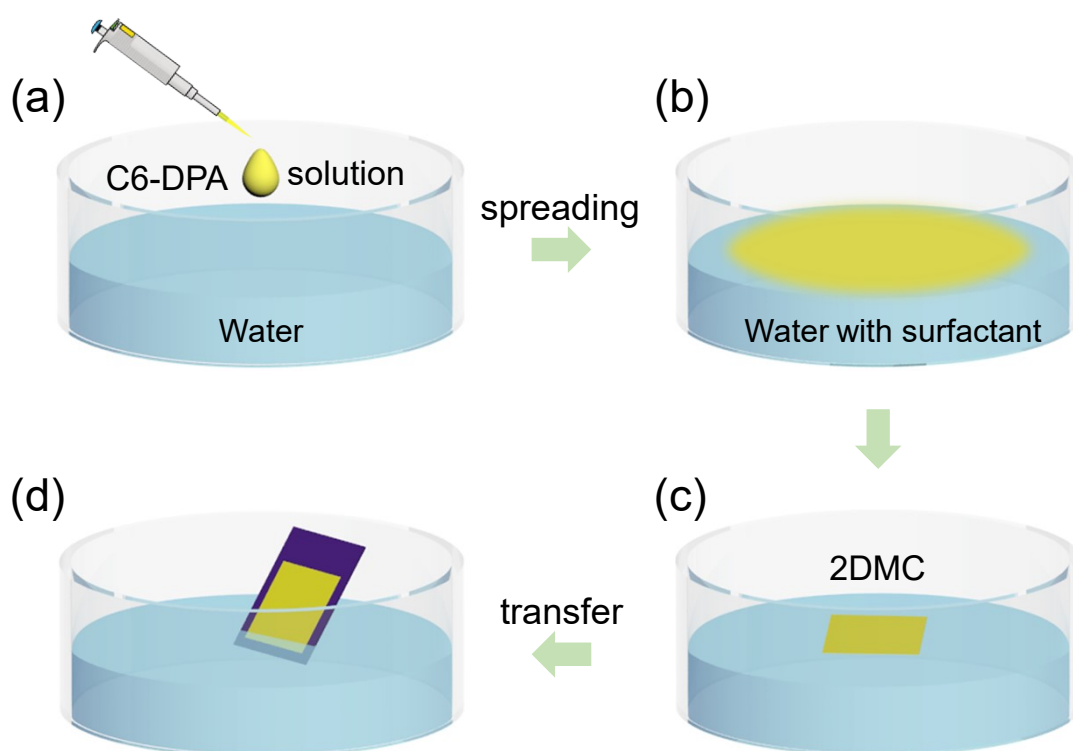

Fig. S1 Schematic illustration of the procedures for the preparation of 2DMCs by the STAS strategy. (a) A low surface tension solution was dropped on the water surface. (b) The solution spread on the water surface. (c) 2DMCs were produced on water surface after solvent evaporation. (d) Transfer of 2DMCs to a target substrate.
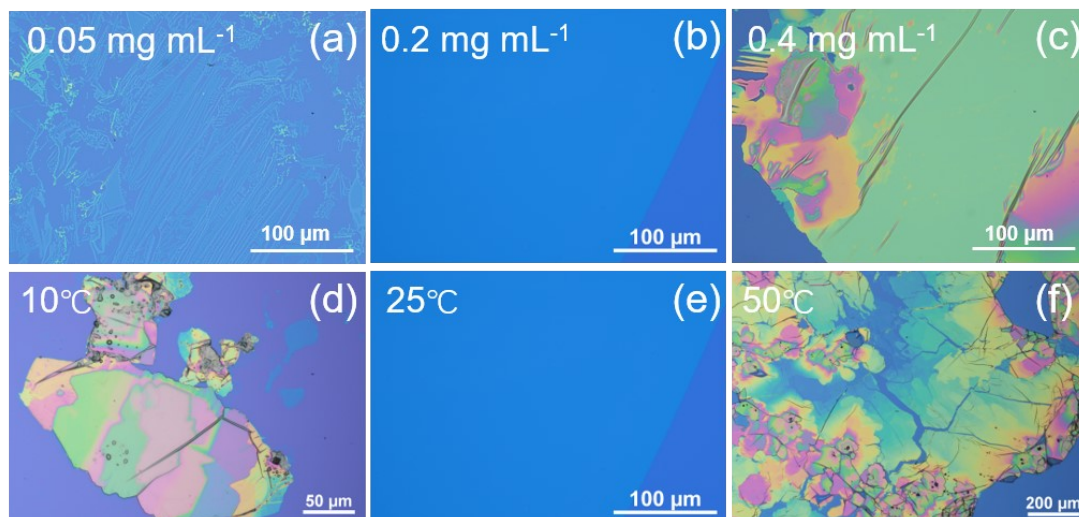
Fig.S2 OM images of C6-DPA 2DMCs obtained at (a-c) different concentrations and (d-f) temperatures. (a) At the low concentration of the organic semiconductor (0.05 mg mL^{-1}), the crystals were discontinuous. (b) At medium concentration of 0.2 mg mL^{-1}, uniform and flat 2DMCs could be obtained. (c) While thick and nonuniform crystals were produced at a high concentration. (d) At low growth temperature of 10°C, thick C6-DPA crystals appeared. (e) At temperature of 25°C, large-area high-quality C6-DPA 2DMCs were obtained. (f) At high temperature of 50°C, the solvent volatilized quickly because of the water temperature was high, resulting in the formation of a large number of discontinuous crystals with uneven thickness. As a result, we used a medium concentration of 0.2 mg mL^{-1} C6-DPA solutuion and a medium growth temperature of 25°C throughout this investigation (unless otherwise stated).
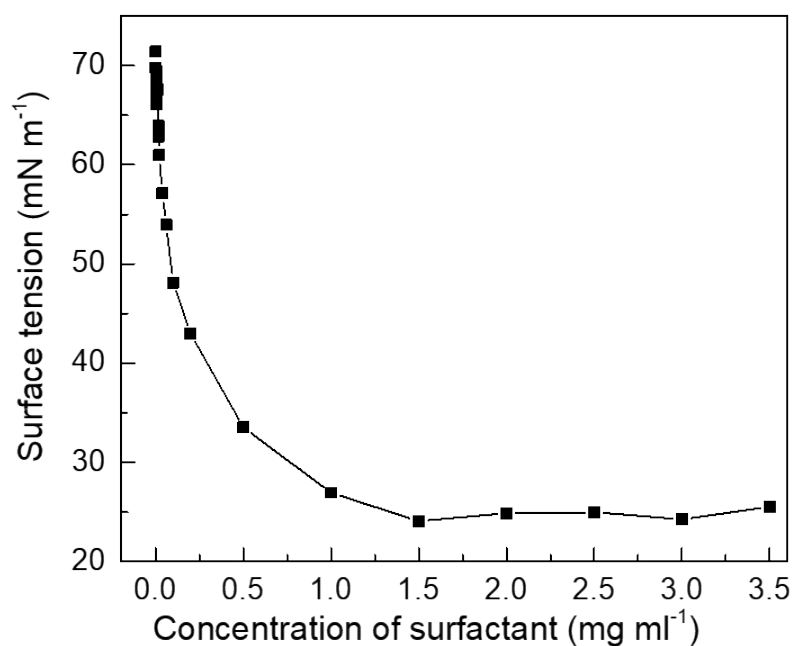
Fig. S3 Surface tension as a function of surfactant concentration. The drastic decrease of surface tension indicated that a surfactant molecular layer formed on water surface.
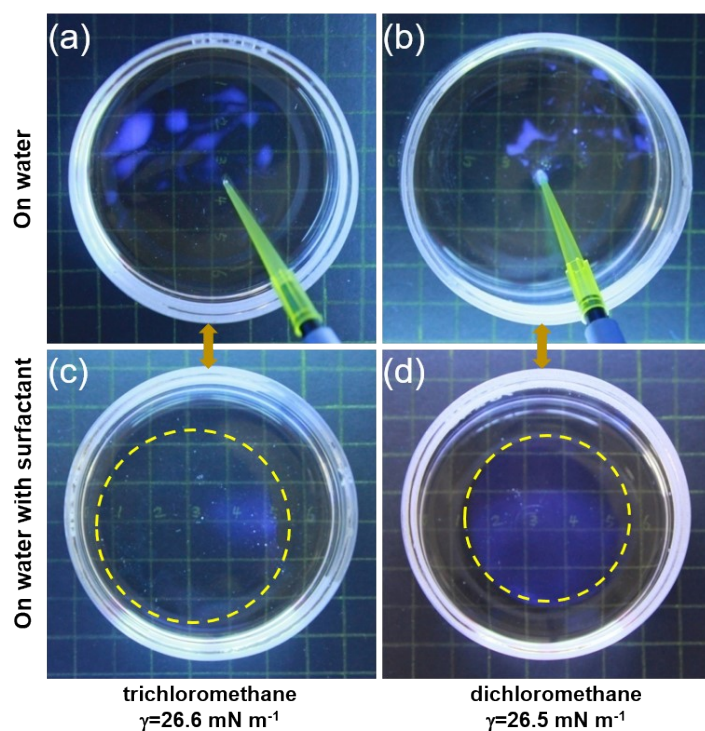

Fig. S4 The spreading of solutions with low surface tension. (a) Trichloromethane and (b) dichloromethane solution separated into small lenses on the pure water surface. In the STAS strategy, the droplet of (c) trichloromethane and (d) dichloromethane solution spread continuously on water surface with the help of the soft template formed by surfactant which was added in the water phase.
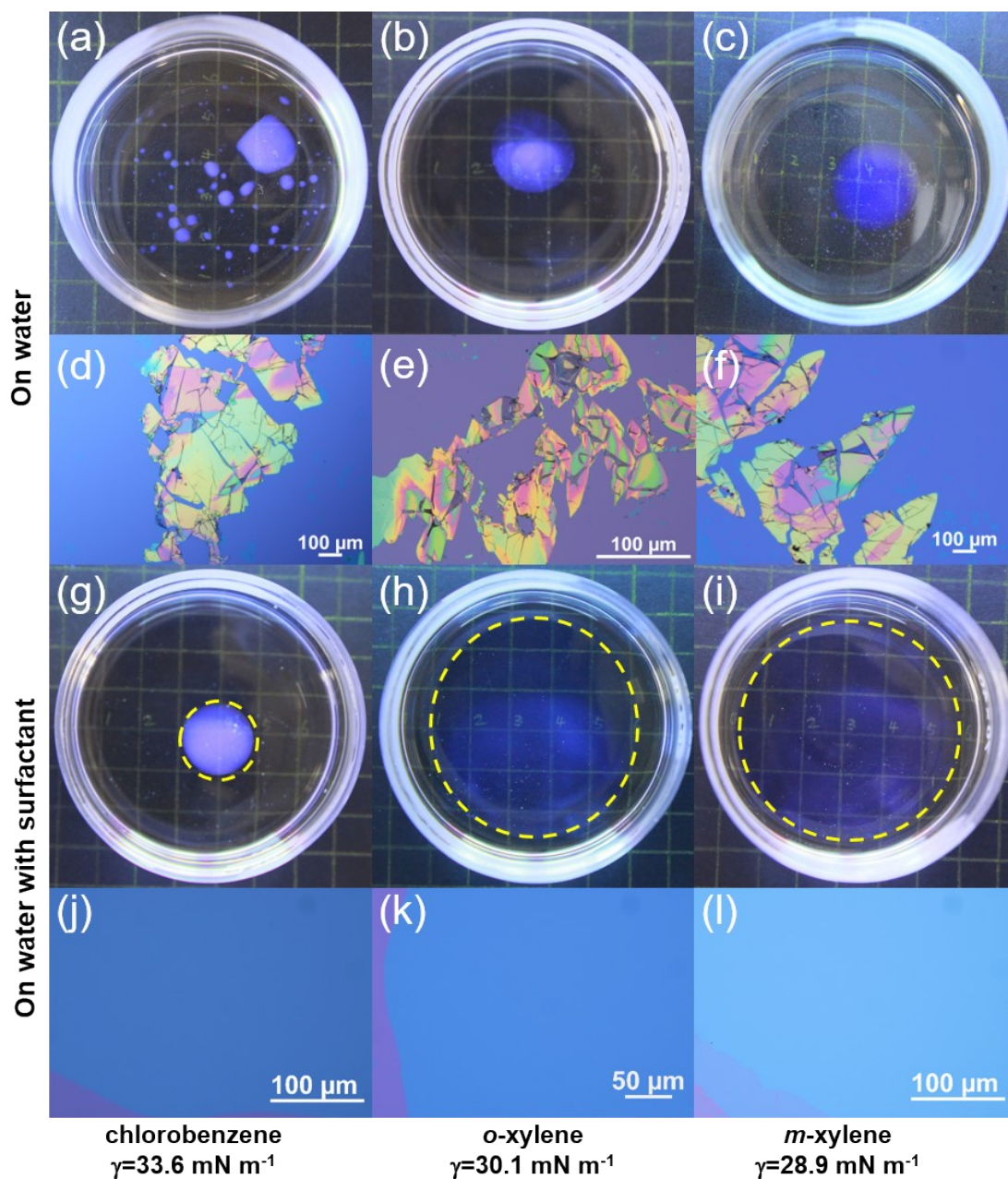
On water

On water with surfactant

| chlorobenzene | *o*-xylene | *m*-xylene |
| $\gamma=33.6$ mN m^{-1} | $\gamma=30.1$ mN m^{-1} | $\gamma=28.9$ mN m^{-1} |

Fig. S5 The spreading of solutions with high surface tension. (a-c) The solution formed small and thick lenses on pure water surface. (d-f) OM images of the crystals grown on the corresponding conditions. (g-i) When surfactant was added into the water, the spreading area of the solution increased significantly, which was conducive to grow large-area 2DMCs. (j-l) OM images of the crystals grown on the corresponding conditions.
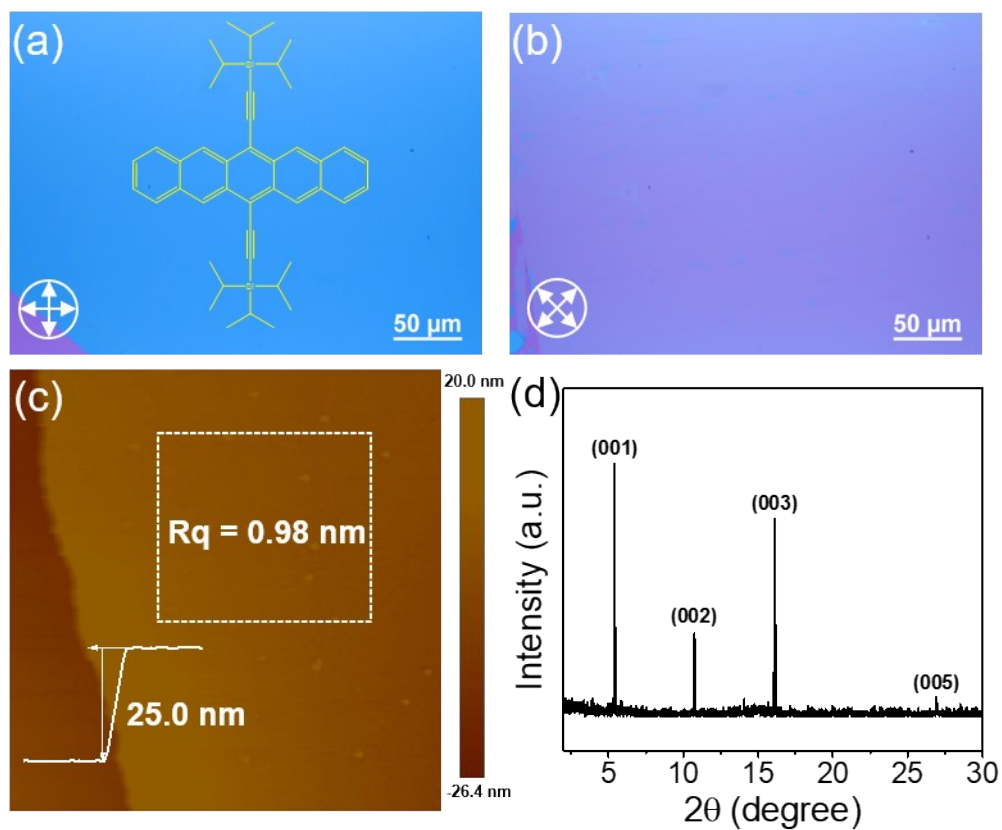
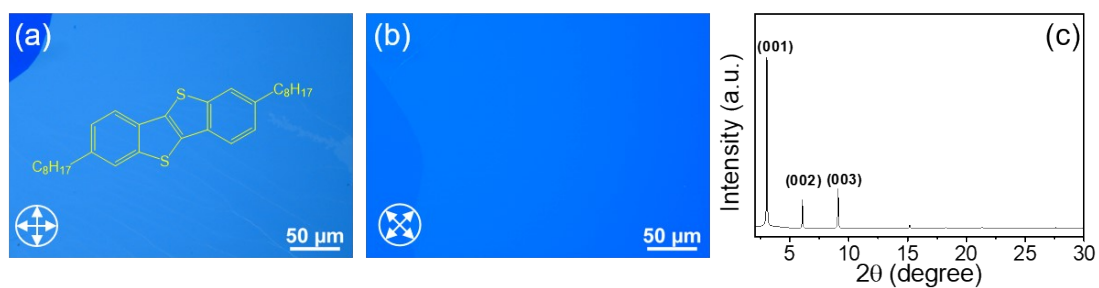**Fig. S6** (a and b) POM images, (c) AFM image and (d) XRD of TIPS-PEN 2DMCs.

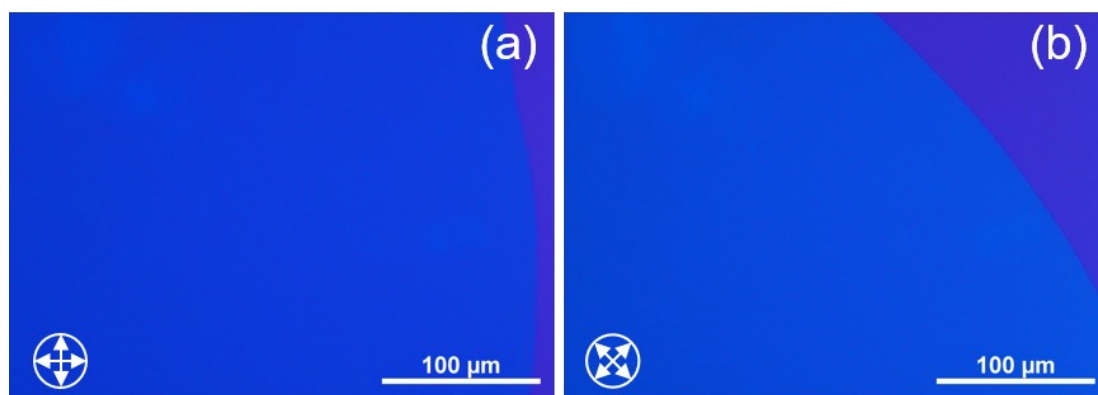**Fig. S7** (a and b) POM images and (c) XRD of C8-BTBT 2DMCs.
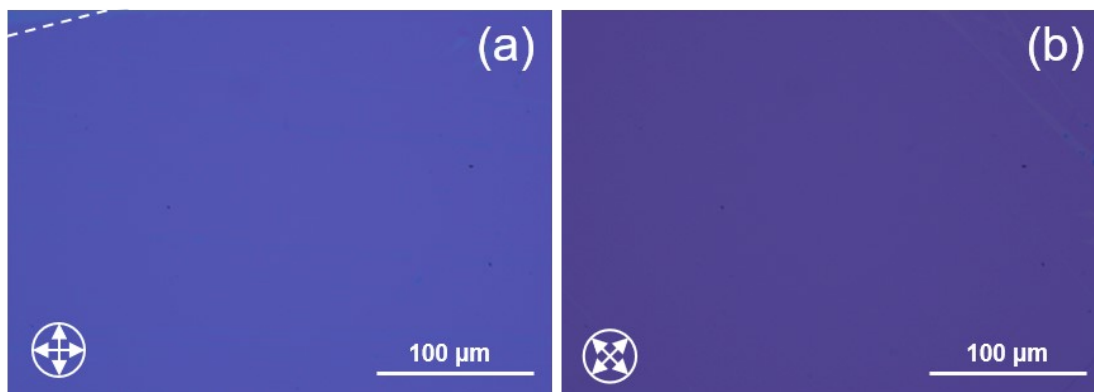

Fig. S8 (a and b) POM images of C6-DPA 2DMCs.

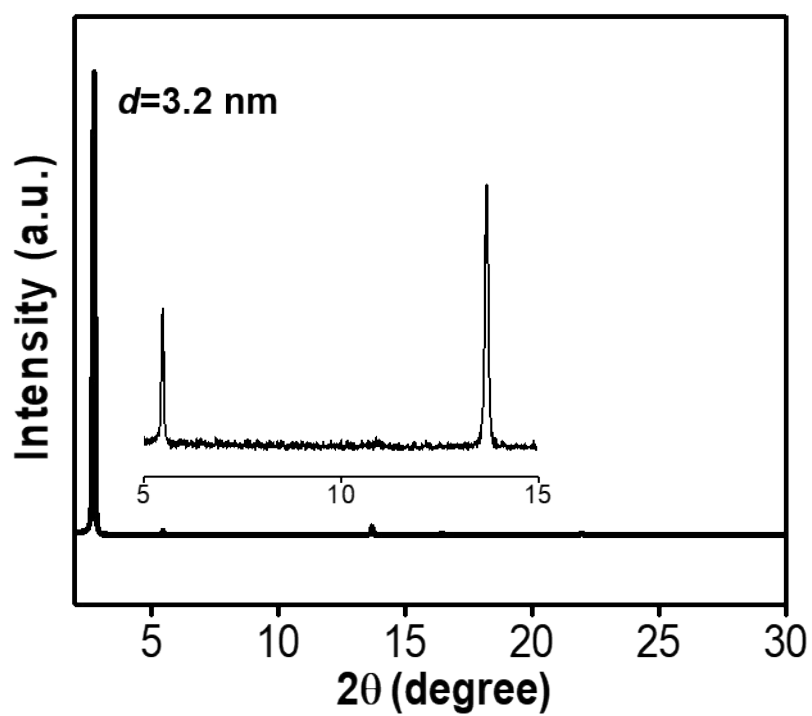**Fig. S9** (a and b) POM images of TFT-CN 2DMCs.
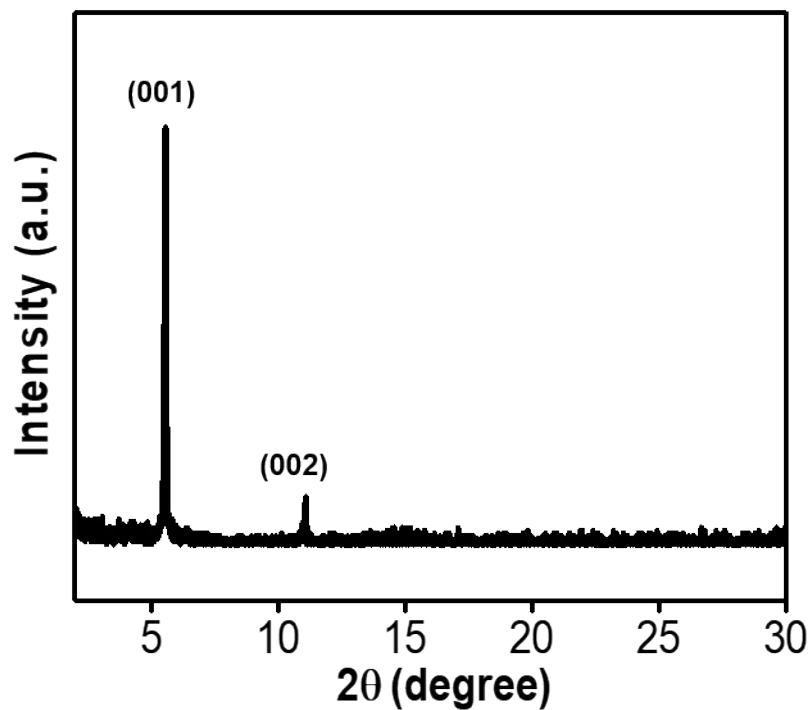

Fig. S10 The XRD of C6-DPA 2DMCs.

Fig. S11 The XRD of TFT-CN 2DMCs.
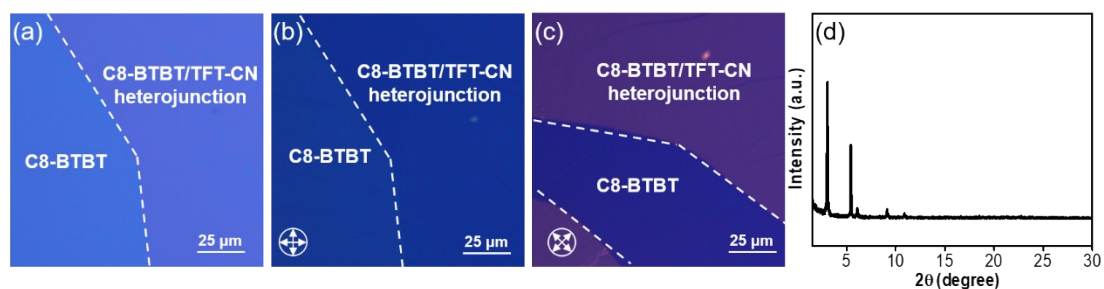
Fig. S12 (a) OM, (b and c) POM images and (d) XRD of heterojunctions based on C8-BTBT and TFT-CN 2DMCs.

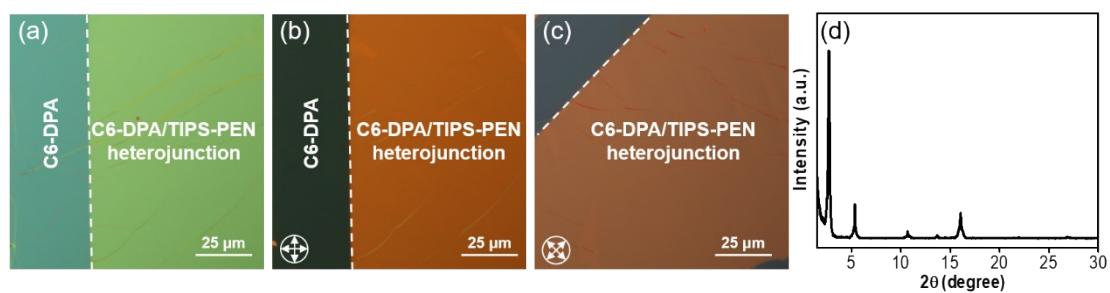**Fig. S13** (a) OM, (b and c) POM images and (d) XRD of heterojunctions based on C6-DPA and TIPS-PEN 2DMCs.
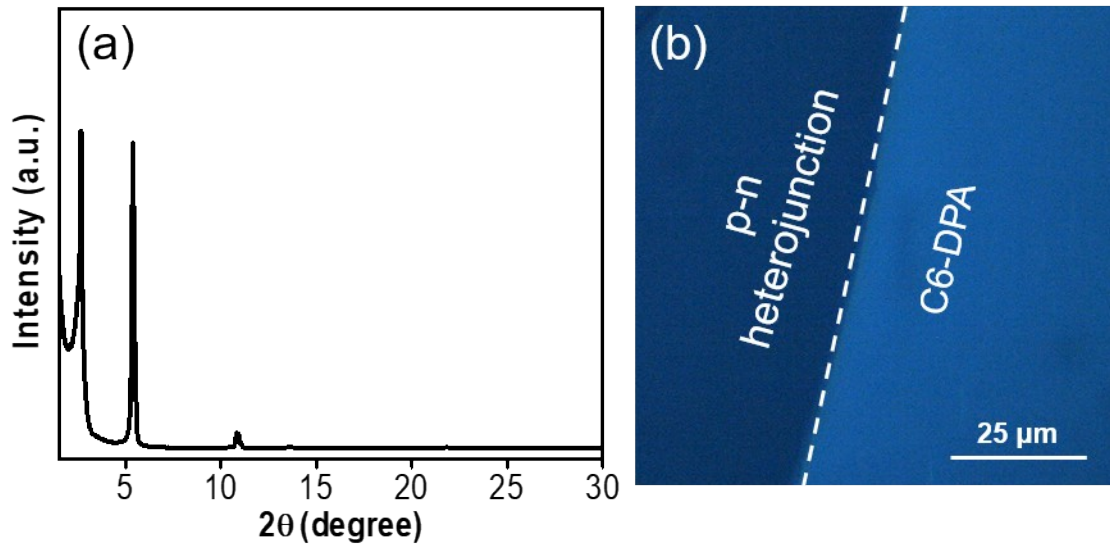
Fig. S14 (a) XRD and (b) fluorescence microscope image of p-n heterojunctions based on C6-DPA and TFT-CN 2DMCs.
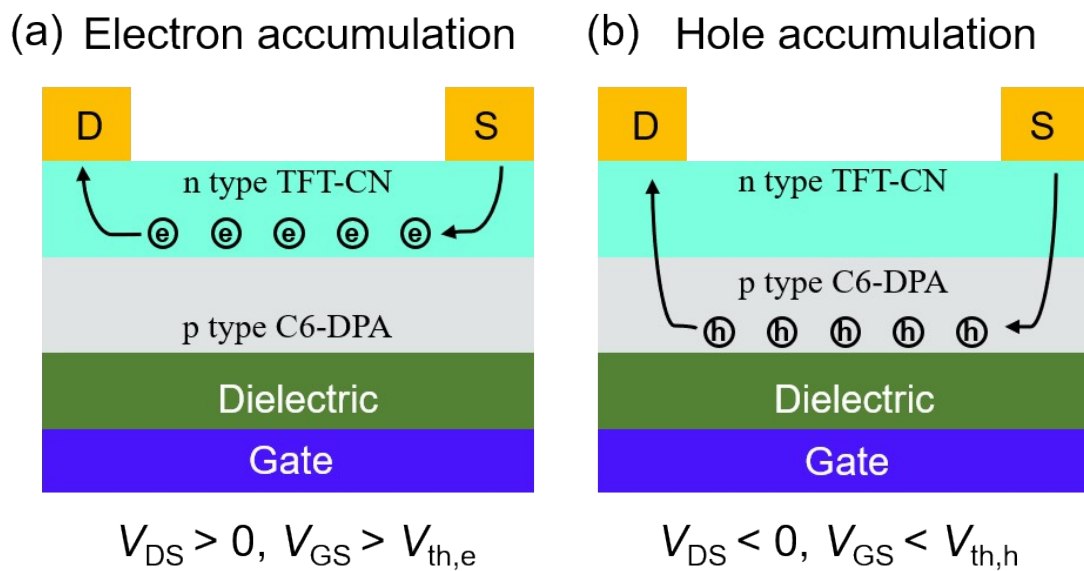

Fig. S15 Schematic illustrations of (a) electron accumulation and (b) hole accumulation model of the aOFETs based on bilayer p–n heterojunctions.

Table S1. Performance comparison of our aOFETs with reported organic single-crystalline aOFETs.

p type materials	n type materials	p-n morphologies	Atmosphere	Max μ_h (cm^2 V^{-1} s^{-1})	Max μ_e (cm^2 V^{-1} s^{-1})	Year	Ref.
CuPc	F$_{16}$CuPc	nanoribbons	N$_2$	0.07	0.05	2010	[4]
C8-BTBT	C$_{60}$	ribbons	air	0.16	0.17	2013	[5]
TIPS-PEN	PTCDI-C8	wire	air	0.23	0.13	2014	[6]
DPP-PR	C$_{60}$	ribbons	N$_2$	0.0061	0.59	2015	[7]
C8-BTBT	TFT-CN	2DMC	air	0.43	0.11	2019	[8]
C6-DPA	TFT-CN	2DMC	air	0.87	0.82	2019	[9]
TIPS-BP	TIPS-TAP	ribbons	N$_2$	1.02	1.90	2019	[10]
C8-BTBT	NDI-C6	2DMC	vacuum	1.40	0.65	2020	[11]
C6-DPA	TFT-CN	2DMC	air	1.96	1.27	2021	[12]
C6-DPA	NDI	2DMC	air	0.54	0.5	2021	[13]
C6-DPA	TFT-CN	2DMC	air	1.50	0.79	This work	

References

1 C. Xu, P. He, J. Liu, A. Cui, H. Dong, Y. Zhen, W. Chen and W. Hu, *Angew. Chem. Int. Ed.*, 2016, **55**, 9519-9523.

2 J. Yao, Y. Zhang, X. Tian, X. Zhang, H. Zhao, X. Zhang, J. Jie, X. Wang, R. Li and W. Hu, *Angew. Chem. Int. Ed.*, 2019, **58**, 16082-16086.

3 C. Wang, X. Ren, C. Xu, B. Fu, R. Wang, X. Zhang, R. Li, H. Li, H. Dong, Y. Zhen, S. Lei, L. Jiang and W. Hu, *Adv. Mater.*, 2018, **30**, 1706260.

4 Y. Zhang, H. Dong, Q. Tang, S. Ferdous, F. Liu, S. C. B. Mannsfeld, W. Hu and A. L. Briseno, *J. Am. Chem. Soc.*, 2010, **132**, 11580-11584.

5 C. Fan, A. P. Zoombelt, H. Jiang, W. Fu, J. Wu, W. Yuan, Y. Wang, H. Li, H. Chen and Z. Bao, *Adv. Mater.*, 2013, **25**, 5762-5766.

6   H. Shim, A. Kumar, H. Cho, D. Yang, A. K. Palai and S. Pyo, *ACS Appl. Mater. Interfaces*, 2014, **6**, 17804-17814.

7   H. Li, C. Fan, W. Fu, H. L. Xin and H. Chen, *Angew. Chem. Int. Ed.*, 2015, **54**, 956-960.

8   L. Wang, C. Wang, X. Yu, L. Zheng, X. Zhang and W. Hu, *Sci. China-Mater.*, 2019, **63**, 122-127.

9   X. Zhu, Y. Zhang, X. Ren, J. Yao, S. Guo, L. Zhang, D. Wang, G. Wang, X. Zhang, R. Li and W. Hu, *Small*, 2019, **15**, 1902187.

10   H. Li, J. Wu, K. Takahashi, J. Ren, R. Wu, H. Cai, J. Wang, H. L. Xin, Q. Miao, H. Yamada, H. Chen and H. Li, *J. Am. Chem. Soc.*, 2019, **141**, 10007-10015.

11   J. Guo, S. Jiang, M. Pei, Y. Xiao, B. Zhang, Q. Wang, Y. Zhu, H. Wang, J. Jie, X. Wang, Y. Shi and Y. Li, *Adv. Electron. Mater.*, 2020, **6**, 2000062.

12   J. Yao, X. Tian, S. Yang, F. Yang, R. Li and W. Hu, *APL Materials*, 2021, **9**, 051108.

13   L. Zheng, C. Wang, X. Tian, X. Zhang, H. Dong and W. Hu, *J. Mater. Chem. C*, 2021, **9**, 472-480.